# Low-frequency coupling between eardrum and manubrium in a finite-element model

W. Robert J. Funnell[a)]
*Departments of BioMedical Engineering and Otolaryngology, McGill University, 3775, rue University, Montréal, QC H3A 2B4, Canada*

(Received 13 March 1995; accepted for publication 7 December 1995)

The mechanical coupling between the eardrum and the manubrium was studied by means of a finite-element model of the cat eardrum. Previous calculations of the effect of varying the eardrum curvature were extended, demonstrating the critical role of curvature in the behavior of the eardrum. A new procedure was developed for directly studying the coupling of forces from different points on the eardrum to the manubrium, and the distribution of load-coupling values over the eardrum surface was calculated. A geometrically simplified eardrum with a circular outline was also studied. It was found that certain regions of the eardrum are more effective in driving the manubrium than can be explained on the basis of their distance from the axis of rotation. This enhanced coupling depends on the curvature of the eardrum but, unlike the mechanism hypothesized by Helmholtz, requires neither tension nor anisotropy. © *1996 Acoustical Society of America.*

PACS numbers: 43.64.Bt, 43.64.Ha

## INTRODUCTION

It has long been accepted that the primary purpose of the middle ear is to function as an impedance-matching transformer between the low-impedance air in the external ear and the high-impedance liquid in the cochlea, but it is not clear just how the transformer ratio is produced. In the present paper this question is investigated by studying the behavior of finite-element models of the eardrum. As in virtually all previous theoretical discussions of the middle-ear transformer ratio, attention is restricted to frequencies lower than a few hundred Hz, low enough for the inertial and damping effects to be negligible.

Helmholtz (1869, 1877) suggested that the eardrum's curvature was the primary cause of the transformer ratio of the middle ear. His theorizing started with the assumption that the eardrum is to be considered a tense membrane. The curved resting shape of the drum, in the absence of any acoustical stimulus, was assumed to be determined by the tension resulting from forces applied to it by the tympanic ring and by the manubrium. Considering a single curved radial fiber, which was assumed to be inextensible, Helmholtz showed how a pressure acting near its center would result in a relatively large displacement at that point but a much smaller displacement at the point of attachment to the manubrium, as though the pressure were acting on the long arm of a lever. The magnitude of the effective lever ratio depended on the precise nature of the curvature of the radial fiber, which in turn was determined by the interaction between the tension and the circular fibers. These circular fibers would need to be extensible, unlike the radial fibers. Their properties would determine the overall shape and the resulting lever ratio. Helmholtz assumed that their properties were such as to produce an optimal shape, and used that shape to estimate an effective lever ratio for a circular eardrum with a small circular disk in place of the manubrium.

Helmholtz' theory received some experimental support 60 years later (Dahmann, 1930), and almost 20 years after that the theory itself was generalized by Esser (1947). Instead of assuming the optimal shape, Esser made various assumptions about the distribution of tension within the membrane and from those assumptions calculated the shape. At about the same time, Guelke and Keen (1949) accepted the essentials of Helmholtz' theory but emphasized the role of the tensor tympani in maintaining the required tension; they also attempted to estimate the actual curvature, and thus the lever ratio, from a photograph of a human eardrum.

Apart from the above authors, however, the idea that the eardrum's curvature played a direct role in the middle ear's transformer ratio was ignored by many authors (Frank, 1923; Fletcher, 1929; Beatty, 1932). The lever action was generally considered to have two components: (a) the ratio of the eardrum area to that of the oval window; and, less importantly, (b) the ratio of the lever arm of the manubrium to that of the long process of the incus. Helmholtz' theory appeared to be completely discredited when Békésy (1941) presented experimental results that he interpreted as meaning that the eardrum vibrates like a hinged plate, with about 65% of its surface area stiffly connected to the manubrium. This mode of vibration would be incompatible with Helmholtz' theory. Békésy also found that the eardrum did not exhibit a significant difference of elasticity between the radial fibers and the circular fibers. Such an anisotropy had been hypothesized by Helmholtz. Furthermore, Wever and Lawrence (1954) were unable to replicate Helmholtz' experiment showing that the average displacement of the eardrum was greater than the concomitant displacement of the manubrium; much later it was shown that Helmholtz' experimental result was apparently wrong as a result of an error in calculation (Hartman, 1971).

The idea that the eardrum vibrates like a hinged plate

[a)]E-mail: funnell@medcor.mcgill.ca



Downloaded 29 Oct 2011 to 132.216.136.181. Redistribution subject to ASA license or copyright; see http://asadl.org/journals/doc/ASALIB-home/info/terms.jsp

was not challenged until the laser-holographic experiments of Khanna and Tonndorf showed that the low-frequency vibration pattern of the eardrum was quite different from that presented by Békésy, for both cat (Khanna and Tonndorf, 1972) and human (Tonndorf and Khanna, 1972). They found that the displacement of the manubrium was smaller than the eardrum displacements on either side of it, and pointed out that that was precisely what would be expected on the basis of Helmholtz' theory about eardrum function.

Finite-element modeling of the eardrum has been successful in reproducing many features of the observed displacements of the cat eardrum (Funnell and Laszlo, 1978; Funnell, 1983; Funnell *et al.*, 1987). In particular, these models have shown that it is possible to reproduce the low-frequency vibration pattern without involving either the tension or the anisotropy that Helmholtz assumed. The fact that the displacement at a point on the eardrum is greater than that on the manubrium does not necessarily mean, however, that there is a useful lever mechanism acting between the two—the force acting at that point on the eardrum might be producing large local displacements simply because the eardrum is flexible, and the force might be having very little influence on the displacement of the manubrium.

The present paper approaches this issue by using a new computational procedure which directly determines the effectiveness with which different points on the eardrum are coupled to the manubrium. This paper also presents an extension of earlier calculations (Funnell and Laszlo, 1978) investigating the effects of changing the shape, and especially the curvature, of the eardrum.

## I. METHODS

### A. Finite-element model

The finite-element model of the cat eardrum presented here is identical to our previous model (Funnell, 1983; Funnell *et al.*, 1987) in most respects. The triangular finite-element mesh is generated with a nominal resolution of 12 elements/diameter (Funnell, 1983). The curvature is defined by a normalized radius of curvature=1.19 (Funnell and Laszlo, 1978). The pars tensa has a thickness of 40 $\mu$m, a Young's modulus of $2\times10^8$ dyn cm$^{-2}$, and a Poisson's ratio of 0.3. The acoustical stimulus is a uniform pressure of 100 dB SPL. The ossicular axis of rotation is fixed, and the combined ossicular and cochlear load is represented by a single lumped rotational stiffness of $14\times10^3$ dyn cm at the axis. There is no acoustical load due to the middle-ear air cavities, that is, the middle-ear septum and bulla are considered to be opened wide. All model displacements presented here are the nodal-displacement components perpendicular to the plane of the tympanic ring—the tympanic ring is in the $x$-$y$ plane and the $z$ components of displacement are calculated.

It has been shown earlier (Funnell, 1983; Funnell *et al.*, 1987; Decraemer *et al.*, 1989) that the behavior of this model compares quite well with experimental results. The low-frequency umbo displacement in the model is approximately 250 nm. Reducing this value by 5 dB to simulate the effect of a closed bulla (Guinan and Peake, 1967) gives about 140 nm, which is only about 3 dB lower than the typical value of 200 nm given by Khanna and Tonndorf (1972) and well within the range of individual variation.

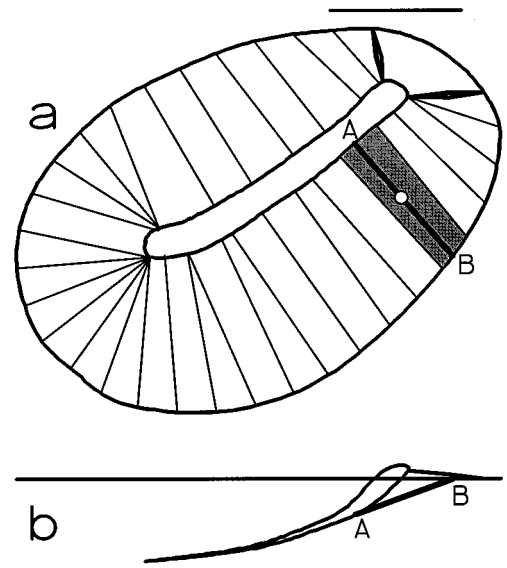


FIG. 1. Procedure for calculating $z$ coordinates using circular arcs. (a) The pars tensa is divided into quadrilateral regions as explained in the text. The open circle represents an internal mesh node for which $z$ is to be determined. Line $AB$ is a straight line from the manubrium to the tympanic ring, passing through the node. The circular arc will lie directly over this line. (b) Side view of the outlines of the tympanic ring and manubrium, again showing the line $AB$.

There are two areas in which this eardrum model differs slightly from our earlier one. The first is in the representation of the manubrium. In our previous models perfect rigidity of the manubrium was obtained by means of a master/slave mechanism (Funnell and Laszlo, 1978). In the present model the manubrium is instead represented by actual elements having finite stiffness. The thicknesses of these elements, and of the elements joining them to the axis of rotation, have been made large enough for them to be practically rigid, and the behavior is equivalent to that in the previous model.

The second, and more important, area of difference is in the procedure for calculating the three-dimensional shape. The basic mechanism is still to define a normalized radius of curvature, $R$, and to use it to determine the $z$ coordinate of each internal node in the finite-element mesh for the pars tensa. The automatic procedure, which was used in our previous models (Funnell and Laszlo, 1978) but which has never been fully described, starts by dividing the surface of the pars tensa into quadrilateral regions by (a) dividing the outer boundary into a number of segments of equal length; and (b) dividing the inner boundary into the same number of segments by locating the inner-boundary point closest to each outer-boundary point. Figure 1(a) shows the resulting quadrilateral regions for the cat eardrum model. To determine the $z$ coordinate for the internal node indicated by an open circle, the first step is to identify the quadrilateral in which the node lies (shaded area). A straight line $AB$ is defined such that (1) its projection onto the plane of the tympanic ring passes through the projection of the node onto that plane; and (2) points $A$ and $B$ divide their respective ends of the quadrilateral in the same proportions. The line



Downloaded 29 Oct 2011 to 132.216.136.181. Redistribution subject to ASA license or copyright; see http://asadl.org/journals/doc/ASALIB-home/info/terms.jsp

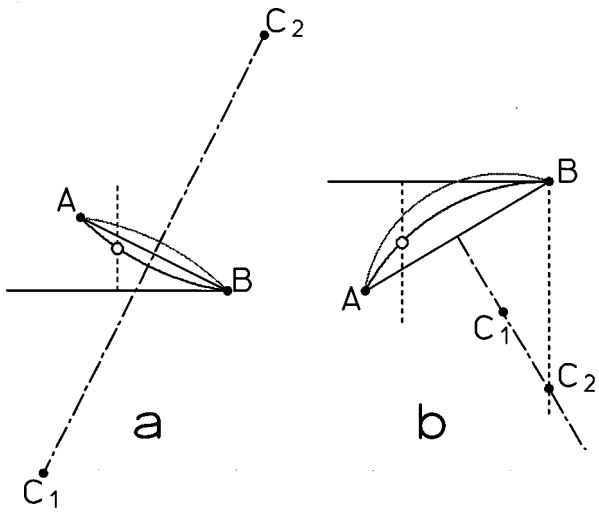


FIG. 2. Handling of two special cases in calculating $z$ coordinates using circular arcs. In each of parts (a) and (b), the horizontal line represents the tympanic ring; $A$ is a point on the manubrium and $B$ is a point on the tympanic ring; $C_1$ and $C_2$ lie on the perpendicular bisector of line $AB$ and are the centers of the circular arcs; and the open circle shows the calculated position of an internal node, at the point of intersection of one of the circular arcs with a vertical dashed line representing the horizontal position of the node. (a) Case where point $A$ is above the tympanic ring, as occurs near the lateral process. By the old method, the center of curvature would have been taken to be below the tympanic ring ($C_1$); with the new method it is taken to be above ($C_2$), giving a more reasonable eardrum shape. (b) Case where the circular arc (center $C_1$) would cross the plane of the tympanic ring. The new center ($C_2$) is taken to be at the intersection of the bisector of line $AB$ with a dashed line through $B$ perpendicular to the tympanic ring.

$AB$ is then treated as the chord of a circular arc. If the length of the chord $AB$ is $l$, and the normalized radius is $R$, then the radius of the arc is given by $r=l\cdot R$. The center of curvature is found by constructing a line which bisects $AB$ and is perpendicular both to $AB$ and to the $x$-$y$ plane, and then locating the point on that line which is distance $r$ from both $A$ and $B$. Once the arc has been defined, the $z$ coordinate of the original node is given as the $z$ coordinate of the arc at the point where it has the same $x$ and $y$ coordinates as the node.

The changes that have now been introduced into this procedure involve the treatment of two special cases, illustrated in Fig. 2. Figure 2(a) shows a case where the point on the manubrium is above the plane of the tympanic ring rather than below. This occurs near the lateral process. In the old method the center of curvature would still be put below the tympanic ring, which results in the rather unrealistic shape shown by the gray arc. In the present model the centre of curvature in this case is put above the tympanic ring, as shown by the solid arc in Fig. 2(a). Figure 2(b) shows a case where the radius of curvature is so small that the arc extends past the level of the tympanic ring, as shown by the gray arc. This can occur (a) because the point on the manubrium is very close to the plane of the tympanic ring; (b) because the chord length $l$ is small so that $r=lR$ is small; or (c) simply because $R$ is small. The first two situations again tend to occur near the lateral process. In the present method, whenever this situation is detected, the software automatically increases $R$ just enough to prevent the arc from crossing the level of the tympanic ring, as shown by the solid arc in Fig. 2(b).

These changes to the handling of the curvature have only small effects on the overall behavior of the model with the usual value of $R=1.19$. In particular, compared with the results of the previous model (Funnell, 1983; Funnell *et al.*, 1987), the new method results in maximal drum displacements and manubrial displacements that are 2% and 3% higher, respectively. The differences are small because the changes affect primarily the part of the pars tensa near the lateral process, where the influence on eardrum and manubrial behavior is relatively slight. The changes are useful, however, in that (a) they produce more reasonable shapes for all values of $R$; and (b) they allow $R$ to be made smaller than previously possible without obtaining absurd shapes, in order to investigate the effects of strong curvatures. Note that, by definition of the normalized radius $R$ as a fraction of the local chord length, the minimum possible value for $R$ is 0.5. In fact, however, the restriction that the circular arc is not allowed to pass the plane of the tympanic ring causes the eardrum shapes to be identical for values of $R$ less than about 0.8 or 0.9 for the eardrum models used here.

### B. Load coupling from eardrum to manubrium

As mentioned above, this paper is restricted to frequencies low enough for there to be no significant inertial or damping forces. The finite-element model thus leads to a matrix equation of the form $\mathbf{Aw}=\mathbf{f}$, where $\mathbf{w}$ is a vector of displacements at the nodes of the model, $\mathbf{f}$ is a vector of forces applied at those nodes, and $\mathbf{A}$ is a symmetric system-stiffness matrix. For each free node in the model there are six components in each of $\mathbf{w}$ and $\mathbf{f}$, representing six degrees of freedom: displacements in the $x$, $y$, and $z$ directions, and rotations about the $x$, $y$, and $z$ axes. Normally, calculation of the displacement pattern of the eardrum is done by calculating a load vector $\mathbf{f}$ corresponding to a uniform pressure applied to the surface of the drum, and then solving the matrix equation for $\mathbf{w}$ using Gaussian elimination and back-substitution.

For the purposes of this paper, it was necessary to calculate the effectiveness of each part of the eardrum in driving the manubrium. This can be done by applying a specified load to every model node, or element, in turn, and calculating the resulting manubrial displacements. Since there are hundreds of nodes and elements in the model, it is clearly not efficient to simply re-solve the matrix equation each time. Therefore the inverse of the system-stiffness matrix was found explicitly, giving the equation $\mathbf{w}=\mathbf{A}^{-1}\mathbf{f}$. For each node or element, the appropriate load vector $\mathbf{f}$ was then determined, and the desired manubrial displacement $w_i$ was calculated by multiplying the $i$th row of $\mathbf{A}^{-1}$ by $\mathbf{f}$.

If it is desired to study the coupling of pressures to the manubrium, the corresponding forces applied to the eardrum must be perpendicular to the eardrum surface. It is possible to calculate the direction of the perpendicular at a particular node by averaging the orientations of the surrounding elements, but this leads to meaningless results at nodes along the boundary between the manubrium and the eardrum where the surface orientation on the two sides of the bound-



Downloaded 29 Oct 2011 to 132.216.136.181. Redistribution subject to ASA license or copyright; see http://asadl.org/journals/doc/ASALIB-home/info/terms.jsp

ary is very different. The local loads were therefore applied on an element-by-element basis—for each triangular element the $x$, $y$, and $z$ components of a force were calculated such that the magnitude of the force was 1 and its direction was perpendicular to the element. These components were then divided equally among the three nodes of that element and inserted into the appropriate locations in **f**. Multiplying **f** by the appropriate row of $\mathbf{A}^{-1}$ then gave the manubrial displacement produced by the force on that element. This manubrial displacement was taken as the coupling value for the element. The results are displayed by superimposing on each element a symbol whose size is proportional to the element's coupling value.

As will be seen below, it is sometimes preferable to study the coupling of forces applied in directions which do not depend on the local orientation of the surface. In these cases the forces were applied on a node-by-node basis rather than an element-by-element basis. The $x$, $y$, and $z$ components of the required force were again inserted into the appropriate locations in **f** and the resulting manubrial displacements were calculated. These nodal coupling values are displayed graphically using contours in the same way that normal eardrum displacement patterns are displayed.

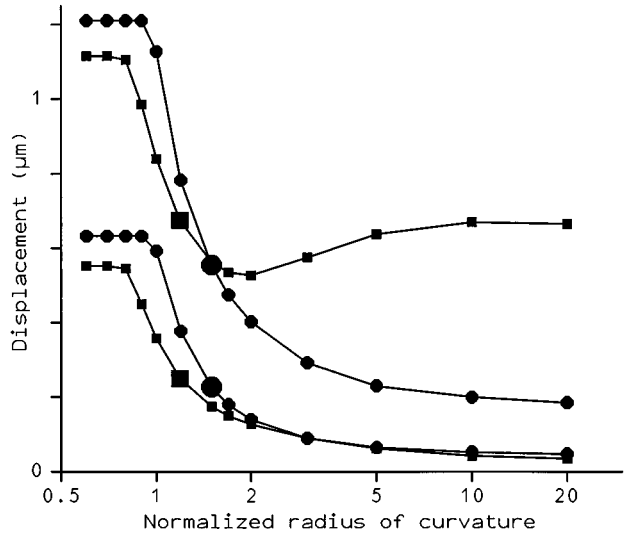


FIG. 3. Model displacements as functions of the normalized radius of curvature $R$. The lower pair of curves represents the displacement of the tip of the manubrium. The upper pair of curves represents the maximal displacement of the eardrum itself. The curves with squares correspond to the CAT model, while the curves with filled circles correspond to the ROUND model. The larger squares and circles correspond to the values of $R$ taken as the ''normal'' values for the two models—1.19 for the CAT model and 1.5 for the ROUND model.

## II. RESULTS

### A. Effects of curvature

Before the element-by-element load-coupling behavior is investigated with the new method described above, it is useful to look at the effects of the curvature on the overall behavior of the eardrum. This can be done by plotting the maximal displacement of the eardrum, and the displacement of the tip of the manubrium, as functions of the normalized radius of curvature $R$.

The lower curve with squares in Fig. 3 represents the displacement of the tip of the manubrium as a function of the normalized radius of curvature $R$. For large values of $R$ the sides of the eardrum are nearly straight, and are very ineffective in transferring perpendicular forces to the manubrium, making the displacements of the latter very small. As $R$ decreases and the sides of the eardrum become more strongly curved, they are better able to apply transverse forces to the manubrium, and the manubrial displacements increase. This is the same behavior as found for an earlier model (Funnell and Laszlo, 1978), although those earlier calculations were limited to values of $R \geqslant 1.19$.

The upper curve with squares in Fig. 3 represents the maximal displacement of the eardrum itself. This curve has a minimum in the region of $R=1$ to 2. There are two principal factors that determine how much the eardrum moves: (a) its bending stiffness, and (b) how much the manubrium moves. For large $R$, since the manubrial displacement is relatively small, the main determinant of drum displacement is drum bending stiffness, which is very small when there is no curvature, and increases as the curvature increases. Thus drum displacement decreases as $R$ decreases from infinity down to about 2. As $R$ becomes smaller than 2, however, the manubrial displacement becomes so large that it becomes the dominant determinant of drum displacement, which thus increases. Note that the shape of the eardrum vibration pattern changes as the degree of curvature changes. As a result, the maximal displacements plotted in Fig. 3 actually occur at different places on the drum for different values of $R$. Figure 4 shows the vibration patterns for four different degrees of curvature—$R=0.9$, 1.19, 2.0, and 5.0. As the radius of curvature increases, the displacement of the manubrium becomes smaller relative to the drum displacements, and the relative amplitudes in the anterior region, above the manubrium, become larger. The location of the maximal eardrum displacement is the same for $R=0.9$ and 1.19, but shifts about 2 mm posteriorly and 1 mm superiorly for $R=2.0$ and then stays there for $R=5.0$.

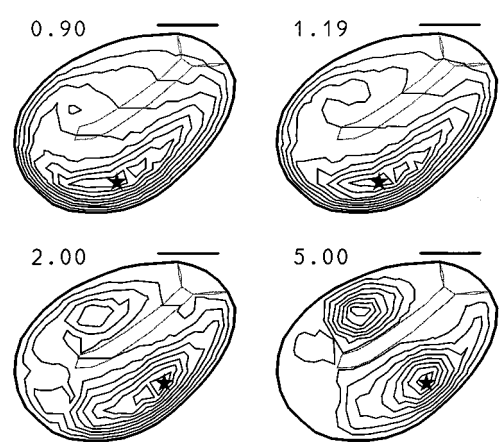


FIG. 4. Vibration patterns of the CAT model for four different degrees of curvature—$R=0.9$, 1.19, 2.0, and 5.0. In each case there are contour lines at ten levels of displacement amplitude, including one at zero and one at the maximum. The position of the maximum displacement for each $R$ is indicated by a star.



Downloaded 29 Oct 2011 to 132.216.136.181. Redistribution subject to ASA license or copyright; see http://asadl.org/journals/doc/ASALIB-home/info/terms.jsp

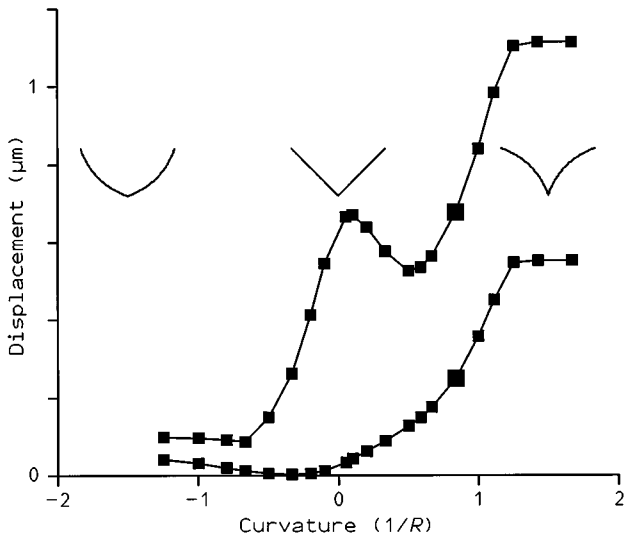


FIG. 5. Displacements in the CAT model as functions of the curvature $1/R$. The lower curve represents the displacement of the tip of the manubrium. The upper curve represents the maximal displacement of the eardrum itself. The larger squares correspond to $R=1.19$. As indicated by the inset diagrams, positive values of $1/R$ correspond to an eardrum whose sides are convex inward, or laterally; negative values correspond to sides which are convex medially; and $1/R=0$ corresponds to straight sides.

It should be noted that the improved coupling of eardrum pressure to the manubrium, due to eardrum curvature, occurs only if the sign of the curvature is such that the sides of the eardrum are concave inward. This is demonstrated in Fig. 5, where the curves of Fig. 3 are replotted as functions of curvature, that is, $1/R$, and then extended to negative values representing an eardrum whose sides are convex medially. It can be seen that for both negative and positive curvatures the maximal eardrum displacement decreases as the curvature becomes nonzero. For negative curvatures, however, the manubrial displacements never become large, and the eardrum displacement continues to drop as the curvature becomes stronger.

### B. Coupling distribution

Figure 6 shows the degree of coupling of different parts of the eardrum to the manubrium. Clearly, the part of the drum which drives the manubrium most effectively is an elongated region inferior to the umbo and extending in the anterior–posterior direction from the umbo almost to the lateral process. There is a zone of reduced coupling between this region and the tympanic ring which is due to the fact that forces here are largely pushing against the immovable tympanic ring. There is another zone of reduced coupling surrounding the manubrium, but the mechanisms involved here are not so straightforward. Because of the asymmetrical shapes of the eardrum and manubrium, it is difficult to analyze the coupling distribution in detail in order to understand its significance.

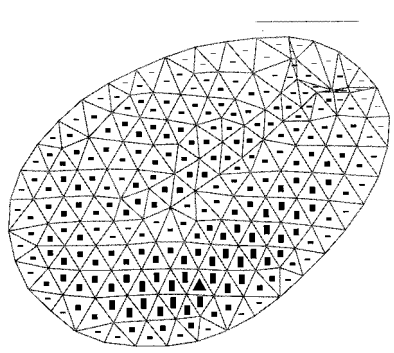

FIG. 6. Distribution of element coupling values for the CAT model. The height of the rectangle in each triangular element is proportional to the manubrial displacement produced by a unit force applied perpendicularly to that element. The filled triangle (▲) indicates the element with the largest degree of coupling.

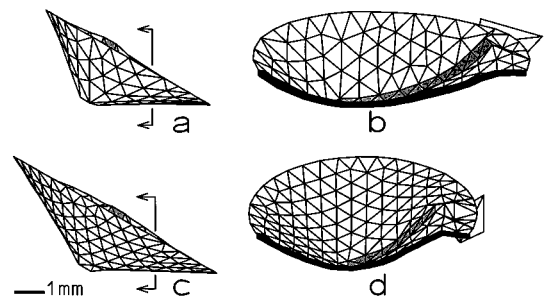


FIG. 7. Comparison of curvatures of CAT and ROUND models which have large values of the normalized radius of curvature $R$. (a) CAT model oriented so that the radial fibers in the posterior region of the pars tensa (where the radial fibers are approximately perpendicular to the long axis of the manubrium) are approximately horizontal and in the plane of the page. (b) CAT model of (a), truncated at the position indicated by the arrows in (a) and then rotated 90° so that the posterior radial fibers are approximately perpendicular to the page. The thick curve shows where the model was truncated. (c) ROUND model oriented as for the CAT model in (a). (d) ROUND model, truncated and rotated as for the CAT model in (b). Note that the sides of the models appear almost straight in both (a) and (c), but that the thick line in (d) is more strongly curved than the thick line in (b).

A geometrically simplified model was created for the purposes of analyzing the coupling values. This new model (hereafter referred to as the ROUND model) has a circular tympanic ring and a symmetrically located manubrium. The $y$ and $z$ coordinates of the axis of rotation, the lateral process, and the umbo, are all the same as in the realistic model (hereafter referred to as the CAT model). The diameter of the eardrum was chosen so that the plane surface area within the tympanic ring (including the pars flaccida, the manubrium, and the ligaments between the pars tensa and pars flaccida) is the same as the corresponding surface area in the CAT model. The lines with filled circles in Fig. 3 represent the behavior of the ROUND model. The lower curve, giving the displacements of the tip of the manubrium, is the same shape as the corresponding curve for the CAT model, but shifted to the right. The upper curve, giving the maximal drum displacement, does not rise for large $R$ because there is still a strong curvature in the circumferential direction, as shown in Fig. 7. This curvature keeps the bending stiffness relatively high.

The distribution of coupling values for pressures—that is, for forces perpendicular to the surface—is interesting since it is by pressures that the eardrum is actually driven, but the analysis of such distributions is complicated by the fact that perpendicular forces applied in different regions have different orientations, which in itself affects how effec-



Downloaded 29 Oct 2011 to 132.216.136.181. Redistribution subject to ASA license or copyright; see http://asadl.org/journals/doc/ASALIB-home/info/terms.jsp

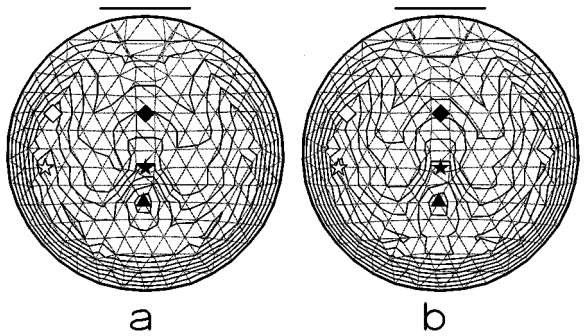


FIG. 8. Distribution of node coupling values for the ROUND model with $R=1.5$. The coupling value of a node is the manubrial displacement produced by a unit force applied to that node. The contours are lines of constant coupling value, from 0% to 100% of the maximum in increments of 10%. The thick lines are the 0% contours, and the filled triangles indicate the positions of the 100% contours, i.e., the positions of the nodes with the largest degree of coupling in each case. The filled stars (⋆) and diamonds (◆) indicate points at the tip of the manubrium and halfway up the manubrium, respectively. The open stars and diamonds indicate the points with maximal coupling values for those vertical positions. (a) Coupling values for nodal forces perpendicular to the plane of the tympanic ring. (b) Coupling values for nodal forces perpendicular to lines joining the nodes to the axis of rotation.

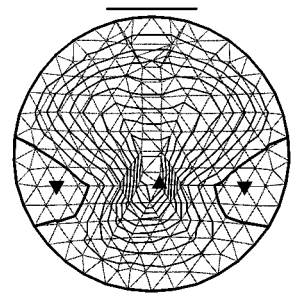

FIG. 9. Distribution of node coupling values for the ROUND model with $R=20$, for nodal forces perpendicular to lines joining the nodes to the axis of rotation. The format is the same as for Fig. 8. The downward-pointing filled triangles (▼) indicate regions of slightly negative coupling values.

tively the forces could drive the manubrium even if they were perfectly coupled to it. The situation can be simplified by applying all the forces perpendicular to the plane of the tympanic ring, that is, parallel to the $z$ axis. Figure 8(a) shows the distribution of nodal coupling values calculated in this way for the ROUND model with $R=1.5$. The distribution is displayed using contour lines of constant coupling value. Here it is seen that the most effective coupling to the manubrium is in a region directly below the umbo. If the degree of coupling of the best-coupled node [indicated by a triangle in Fig. 8(a)] is taken as 100%, then the node at the tip of the manubrium itself (indicated by a filled star) has a relative coupling value of about 65%. The lower effectiveness of the node at the tip might be explained simply by the fact that it is closer to the axis of rotation. However, the distance of the tip from the axis is in fact roughly 75% of that of the best-coupled element, so the tip coupling value is significantly less than would be predicted solely on the basis of its distance from the axis of rotation. This indicates that the best-coupled element, in addition to being further from the axis, has an additional mechanical advantage.

The largest coupling value at the level of the tip of the manubrium is found to be over 70%, at the position indicated by an open star. This coupling value is somewhat larger than the value at the tip of the manubrium, so here again is a case where the coupling of the node to the manubrium is greater than can be explained by its distance from the axis of rotation. Even larger differences are found for nodes closer to the axis of rotation—the manubrial nodes about halfway up the manubrium (filled diamond) have coupling values of about 40%, while the coupling values on the eardrum at the same level reach more than 60% (open diamond). The fact that there is not a simple rigid coupling of the drum to the manubrium is further attested by the fact that the nodes in the region close to the manubrium have considerably smaller coupling values than those on the manubrium. For example, the node immediately to the left of the manubrial tip has a coupling value of about 40%, compared with about 65% on the manubrium.

The use of forces parallel to the $z$ axis to calculate the coupling values avoids the surface-orientation problems involved with pressures, and is also attractive since it might be feasible to do the equivalent experiment on a real eardrum. There is still, however, a complication due to the geometry of the eardrum. In the present model the ossicular axis of rotation and the tympanic ring are both in the $x$-$y$ plane. Since a node near the outside of the eardrum is close to this plane, a line drawn from the node to the axis of rotation will be almost perpendicular to the $z$ axis, and a force applied at that node parallel to the $z$ axis will be well oriented for producing a torque around the axis of rotation. For a node further from the outside, however, there will be a smaller angle $\theta$ between the $z$ axis and a line drawn from the node to the axis of rotation. If a force parallel to the $z$ axis is applied at the node, its effectiveness in applying a torque around the axis of rotation will be reduced by a factor equal to the cosine of the angle $\theta$. This would result in reduced coupling values for nodes on or near the manubrium. To avoid this effect, one can replace the nodal force which was always parallel to the $z$ axis with one which is perpendicular to a line drawn from the node to the axis of rotation. Figure 8(b) presents coupling values calculated in this way. The tip of the manubrium now has a coupling value of about 75% while the coupling values on the eardrum at the same level reach over 80%. Halfway up the manubrium the coupling value is close to 50% while the values on the eardrum at the same level reach 70%. It thus appears that some nodes on the eardrum have coupling values that are as much as 1.5 times as large as can be explained on the basis of their distances from the axis of rotation.

The fact that the enhanced coupling of some eardrum regions is related to the eardrum's curvature is seen by examining the behavior of a model which has very little curvature. Figure 9 shows the distribution of coupling values for a model with $R=20$, that is, with sides that are almost completely straight in the radial direction. It is seen that no element has a coupling value which is significantly higher than that of a manubrial element at the same distance from the axis of rotation.



Downloaded 29 Oct 2011 to 132.216.136.181. Redistribution subject to ASA license or copyright; see http://asadl.org/journals/doc/ASALIB-home/info/terms.jsp

## III. DISCUSSION

As used in mechanics and acoustics, the term *membrane* refers to a thin sheetlike structure under tension where the transverse stiffness is due almost entirely to the tension, and the bending stiffness of the material itself is negligible. The term *plate*, in contrast, refers to the case where the bending stiffness of the material is significant, and where there may be no tension at all (Kinsler and Frey, 1962). A *shell* is defined as a plate which is not flat—the curvature of a shell dramatically increases its effective bending stiffness. It is important to emphasize that the same sheet of a given material can act as a plate, a shell or a membrane, depending on the applied boundary conditions.

Helmholtz thought of the eardrum as a membrane whose curvature, in the absence of significant inherent bending stiffness, would be determined purely by the interaction of the tension with the three-dimensional geometry and with the longitudinal stiffnesses of the membrane's fibers. Discussion of the curvature-lever idea has always been in terms of the membrane model (Békésy, 1941; Esser, 1947; Guelke and Keen, 1949; Marquet *et al.*, 1973; Tonndorf and Khanna, 1972; Rabbitt and Holmes, 1986). The essential feature of the curvature-lever mechanism, however, is the curvature, not whether the structure is a membrane or not. As the present finite-element results show, a shell model is also capable of demonstrating a curvature-related force amplification.

Two factors that are of prime importance in a membrane model of the eardrum are tension and anisotropy. The shell eardrum model presented here has neither, and clearly neither is required to produce a curvature-related force amplification. This does not necessarily mean, however, that neither occurs in the real eardrum, and one recent quantitative eardrum model includes both (Rabbitt and Holmes, 1986). There is no good direct experimental evidence for tension in the resting eardrum (Funnell and Laszlo, 1982), but clearly there will be tension at least when the tensor tympani muscle is contracting. It is not clear how this would affect the curvature-related force amplification. With respect to anisotropy, the eardrum is anatomically anisotropic and appears to exhibit different strengths in the radial and circumferential directions (Békésy, 1941; Yamamoto *et al.*, 1990), but the stiffness does not appear to be strongly anisotropic (Funnell and Laszlo, 1982). The anatomical anisotropy may affect the in-plane properties of the eardrum differently than it affects the bending properties (Rabbitt and Holmes, 1986). It has been shown with the shell model (Funnell and Laszlo, 1978) that the coupling between the eardrum and the manubrium would be enhanced if the stiffness in the circumferential direction were less than that in the radial direction.

It is important to remember that the fact that the ratio of average eardrum displacement to manubrial tip displacement is less than 1 (Wever and Lawrence, 1954; Hartman, 1971) does not in itself refute Helmholtz' curved-membrane lever-ratio hypothesis. What it does imply is that the curvature-related lever ratio is smaller than Helmholtz thought (Tonndorf and Khanna, 1972). As was recognized by Helmholtz himself, a complete analysis of the force transformations of the eardrum must take into account a great many interacting factors. It may be helpful to think in terms of three different mechanisms—eardrum/footplate area ratio, ossicular lever-arm ratio, and curvature-related transformation ratio. It is difficult, however, to meaningfully separate the force-transformation behavior into these distinct mechanisms: the effective surface area of the eardrum depends on the displacement distribution, and this and the curvature-related lever mechanism both depend on the geometry and material properties in interrelated ways. What does seem clear is that all three types of mechanism (as well as the effects of inertia and damping at higher frequencies) are involved in determining the characteristics of the overall pressure-to-force transformation. Furthermore, the curvature of the eardrum is important not only in producing an additional Helmholtz-type of lever ratio but, more importantly, in largely determining the effective overall stiffness of the eardrum.

## ACKNOWLEDGMENTS

This work was supported by the Medical Research Council of Canada. I thank J. Lauzière for editing the manuscript.

Beatty, R. T. (**1932**). *Hearing in Man and Animals* (Bell, London), pp. 5–6.

Békésy, G. v. (**1941**). ''Über die Messung der Schwingungsamplitude der Gehörknöchelchen mittels einer kapazitiven Sonde,'' Akust. Z. **6**, 1–16. English translation: Békésy, G. v. (**1960**). *Experiments in Hearing* (McGraw-Hill, New York), pp. 95–104.

Dahmann, H. (**1930**). ''Zur Physiologie des Hörens; experimentelle Untersuchungen über die Mechanik der Gehörknöchelchenkette sowie über deren Verhalten auf Ton und Luftdruck,'' Z. Hals Nasen Ohrenheilkd. **27**, 329–368.

Decraemer, W. F., Khanna, S. M., and Funnell, W. R. J. (**1989**). ''Interferometric measurement of the amplitude and phase of tympanic membrane vibrations in cat,'' Hear. Res. **38**, 1–18.

Esser, M. H. M. (**1947**). ''The mechanism of the middle ear: II. The drum,'' Bull. Math. Biophys. **9**, 75–91.

Fletcher, H. (**1929**). *Speech and Hearing* (Van Nostrand, New York), p. 116.

Frank, O. (**1923**). ''Die Leitung des Schalles im Ohr,'' Sitzungsber, Math.-Phys. Kl. Bayer. Akad. Wiss. (München) 11–77.

Funnell, W. R. J. (**1983**). ''On the undamped natural frequencies and mode shapes of a finite-element model of the cat eardrum,'' J. Acoust. Soc. Am. **73**, 1657–1661.

Funnell, W. R. J., and Laszlo, C. A. (**1978**). ''Modeling of the cat eardrum as a thin shell using the finite-element method,'' J. Acoust. Soc. Am. **63**, 1461–1467.

Funnell, W. R. J., and Laszlo, C. A. (**1982**). ''A critical review of experimental observations on ear-drum structure and function,'' ORL **44**, 181–205.

Funnell, W. R. J., Decraemer, W. F., and Khanna, S. M. (**1987**). ''On the damped frequency response of a finite-element model of the cat eardrum,'' J. Acoust. Soc. Am. **81**, 1851–1859.

Guelke, R., and Keen, J. A. (**1949**). ''A study of the vibrations of the tympanic membrane under direct vision, with a new explanation of their physical characteristics,'' J. Physiol. **110**, 226–236.

Guinan, J. J., Jr., and Peake, W. T. (**1967**). ''Middle ear characteristics of anesthetized cats,'' J. Acoust. Soc. Am. **41**, 1237–1261.

Hartman, W. (**1971**). ''An error in Helmholtz's calculation of the displacement of the tympanic membrane,'' J. Acoust. Soc. Am. **49**, 1317.

Helmholtz, H. F. L. (**1869**). ''Die Mechanik der Gehörknöchelchen und des Trommelfells,'' Pflügers Archiv. Physiol. **1**, 1–60. English translations—(1) Bucks, A. H., and Smith, N. (transls.) (**1873**). *The Mechanism of the Ossicles of the Ear and Membrana Tympani* (Woods, New York), 69 pp.



Downloaded 29 Oct 2011 to 132.216.136.181. Redistribution subject to ASA license or copyright; see http://asadl.org/journals/doc/ASALIB-home/info/terms.jsp

(2) Hilton, J. (transl.) (**1874**). *The Mechanism of the Ossicles and the Membrana Tympani*, (New Sydenham Society, London), Vol. 62, pp. 97–155.

Helmholtz, H. L. F. (**1877**). *Die Lehre von den Tonempfindungen* (Verlag von Fr. Vieweg u. Sohn, Braunschweig), 4th ed. English translation—Ellis, A. J. (transl.) (**1885**). *Sensations of Tone* (Longmans, Green & Co., London), 2nd ed. Reprinted (**1954**). (Dover, New York), pp. 134–135.

Khanna, S. M., and Tonndorf, J. (**1972**). ''Tympanic membrane vibrations in cats studied by time-averaged holography,'' J. Acoust. Soc. Am. **51**, 1904–1920.

Kinsler, L. E., and Frey, A. R. (**1962**). *Fundamentals of Acoustics* (Wiley, New York), 2nd ed., p. 81.

Marquet, J., van Camp, K. J., Creten, W. L., Decraemer, W. F., Wolff, H. B., and Schepens, P. (**1973**). ''Topics in physics and middle ear surgery,'' Acta Oto-Rhino-Laryngol. Belg. **27**, 137–320.

Rabbitt, R. D., and Holmes, M. H. (**1986**). ''A fibrous dynamic continuum model of the tympanic membrane,'' J. Acoust. Soc. Am. **80**, 1716–1728.

Tonndorf, J., and Khanna, S. M. (**1972**). ''Tympanic membrane vibrations in human cadaver ears studied by time-averaged holography,'' J. Acoust. Soc. Am. **52**, 1221–1233.

Wever, E. G., and Lawrence, M. (**1954**). *Physiological Acoustics* (Princeton U. P., Princeton), pp. 86–89.

Yamamoto, N., Ishii, T., and Machida, T. (**1990**). ''Measurement of the mechanical properties of the tympanic membrane with a microtension tester,'' Acta Otolaryngol. **110**, 85–91.



Downloaded 29 Oct 2011 to 132.216.136.181. Redistribution subject to ASA license or copyright; see http://asadl.org/journals/doc/ASALIB-home/info/terms.jsp